Reprinted from: J.C.J. Nihoul and B.M. Jamart (Editors)
Three-Dimensional Models of Marine and Estuarine Dynamics, pp. 169—194



# DYNAMICS OF AGULHAS RETROFLECTION AND RING FORMATION IN A QUASI-ISOPYCNIC COORDINATE NUMERICAL MODEL

E.P. CHASSIGNET AND D.B. BOUDRA
Rosenstiel School of Marine and Atmospheric Science, University of Miami, 4600 Rickenbacker Causeway, Miami FL 33149-1098, (USA)

## ABSTRACT

The Agulhas retroflection region of the idealized South Atlantic-Indian ocean model described by De Ruijter and Boudra (1985) and Boudra and de Ruijter (1986) is analyzed in detail. First, the physical mechanism of the model retroflection is presented through illustration of the Agulhas' vorticity balance among various experiments, and second, the ring formation process is described in terms of its vertical structure and the associated energy conversions.

Analysis of the vorticity balance in a one-layer model shows that both inertia and internal friction may account for a partial retroflection where a linear, weakly viscous system has none. In a series of one-, two-, and three-layer nonlinear, weakly viscous experiments, it is shown that retroflection is accomplished through a free inertial boundary layer, as suggested originally by De Ruijter (1982), and, furthermore, that it is the planetary vorticity advection, rather than the inertial overshooting distance, which is of greatest importance. Halving horizontal grid spacing (from 40 to 20 km) is shown to have a minor impact on the vorticity balance and the retroflection strength. The importance of a substantial viscous stress curl along the coast of Africa, as provided by the no-slip condition, is illustrated through comparison with a slippery Africa experiment. Because of the apparent importance of the planetary vorticity advection in the retroflection regime, an experiment with a more realistic South African coastal geometry is described. It is shown that the retroflection is still strong but that the associated recirculation is less intense. The primary terms of the vorticity equation have smaller magnitude but they exhibit the same basic balance as in the nonlinear, weakly viscous, rectangular Africa experiments: between planetary vorticity advection and viscous stress curl along the coast, and between planetary and relative vorticity advection on the seaward side of the coastal Agulhas and elsewhere throughout the retroflection.

The mean energetics of the experiments are examined in order to gain additional understanding of the model retroflection. Also, the signatures of barotropic and baroclinic instability in the ring formation process for three experiments are studied in detail using eddy-mean energetics. Ring formation is accompanied by development of a pronounced cyclonic circulation in the lower layer. However, both barotropic and baroclinic conversions reach a maximum at the moment of ring cutoff. Therefore, a mixed instability is suggested.

## 1 INTRODUCTION

One of the most intriguing features in world ocean circulation is the retroflection of the Agulhas Current south of Africa, and an important phenomena associated with it is ring formation at its western edge. The Agulhas constitutes the primary boundary current of the southwestern Indian Ocean, and as it separates from the southern tip of Africa in a southerly or southwesterly direction, the major part of it retroflects, returning eastward to rejoin the subtropical gyre. Several times a year, in retroflecting, the current cuts itself off and a ring of warm, salty Indian Ocean water is formed. These rings drift westward and, along with other leakage of Agulhas water around the tip of Africa, likely have an important impact on the heat and salt budget of the South Atlantic.

In this paper, we present some basic dynamical ideas and numerical results concerning the Agulhas retroflection and the ring formation. The dynamical topics include, 1) the retroflection vorticity balance, 2) the mean energetics and 3) the nature of the instability associated with ring formation.

## 2 DESCRIPTION OF THE MODEL AND THE EXPERIMENTS

The numerical models used are described in De Ruijter and Boudra (1985) and Boudra and de Ruijter (1986)(henceforth referred to as DB and BD, respectively). The authors included temporal variability, friction, inertia and the beta-effect in a study of the South Atlantic-Indian Ocean circulation, using first a one-layer simplification of, and then the full quasi-isopycnic coordinate numerical model of Bleck and Boudra (1981). Perhaps overly idealized aspects of

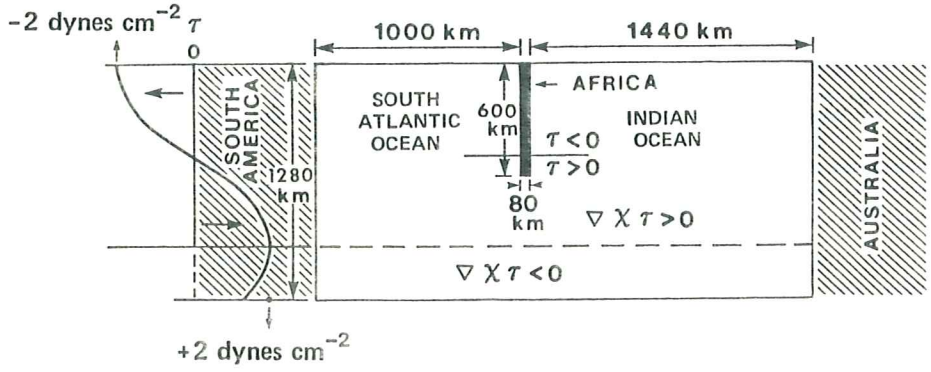


Fig.1. Geometry of the flat bottom ocean basin used in all the numerical experiments, except E11. The wind stress profile is shown at the left.

their model were the simple rectangular shape for Africa and the small total basin size. In DB and BD, the primary focus was on parameters affecting the exchange of fluid between the two basins. It was surmised that the no-slip African coast and the magnitude of the planetary vorticity advection at separation figured prominently in the retroflection vorticity balance. Influence of several other model parameters among their experiments, including internal lateral friction, horizontal resolution, stratification, incorporation of bottom drag, and interaction with the other wind-driven currents, were also examined.

The parameters for the experiments discussed in this study are presented in Table 1. Many of these are experiments discussed in DB and BD, but several new

TABLE 1

Parameters for the experiments discussed in this study.
Blanks indicate no change from the previous experiment.

| Experiment | LIN1 | NLIN1 | LIN2 | NLIN2 | E1 | E2 | E3 | E8 | E9 | E10 | E11 |
|---|---|---|---|---|---|---|---|---|---|---|---|
| Nonlinear terms | NO | YES | NO | YES | | | | | | | |
| Number of layers | 1 | | | | 2 | 3 | | | | | |
| Thickness of the layers (m) | 1000 | | | | 1000<br>4000 | 600<br>700<br>3700 | 300<br>900<br>3800 | | | | |
| g'($ms^{-2}$) | | | | | .02<br>.005 | .02<br>.005 | | | | | |
| Viscosity ($m^2s^{-1}$) | 330 | | 3300 | | 330 | | | | | | |
| Bottom drag coeff. ($s^{-1}$) | | | | | | | | $10^{-7}$ | | | |
| Boundary conditions on Africa[1] | NS | | | | | | | | FS | NS | |
| Horizontal resolution (km) | 40 | | | | | | | | | 20 | |
| Africa's geometry[2] | A | | | | | | | | | | B |

[1] NS=No-slip; FS=Free-slip [2] A=Rectangular (Fig. 1); B=More realistic (Fig.5)

ones have been introduced to clarify aspects of the vorticity balance and one to give the Beta-effect more realistic importance. The basin used in the experiments is described in DB and BD, but is illustrated here for convenience (Fig.1). The steady wind stress profile is shown at the left of the figure. The direct effect of the wind stress decreases linearly from its maximum near the surface to zero at a pressure of 100 db. In the multilayer cases, the wind forcing is therefore partitioned among the top two layers if the upper layer thickness becomes less than 100 db. The conditions on meridional boundaries are generally no-slip (u=v=0) and those for zonal boundaries free-slip (v=du/dy=0), except in one experiment where the coast of Africa is treated homogeneously as a free-slip boundary. The character of retroflection and ring formation in the experiments is summarized in Table 2.

TABLE 2

Description of the upper layer flow pattern of the model retroflection region

| | |
|---|---|
| LIN1 | Small recirculation cell east of Africa. Most of the flow (35 Sv) goes into the Atlantic. |
| NLIN1 | Substantial retroflection extending southwest of the tip of Africa. Approx. 15 Sv leakage into the Atlantic. High temporal variability. |
| LIN2 | Establishment of a retroflection but with 20-25 Sv leakage. |
| NLIN2 | Similar to LIN2. The retroflection is moved south and west of the tip of Africa. Steady solution. |
| E1 | Similar to NLIN1, but with 25 Sv leakage and less variability. Rings are formed continuously at a rate of about 5 per year. |
| E2 | Similar to E1, but with 15 Sv leakage and the position of the retroflection closer to the tip of Africa. The rate of ring formation is about 4 per year. |
| E3 | The current retroflects very soon after it separates from the coast. Small leakage (less than 5 Sv). High eddy energy in the retroflection. No rings. |
| E8 | Similar to E3, but the circulation is more intense. No rings. |
| E9 | Most of the flow turns westward and then northward along the coast into the Atlantic. |
| E10 | Similar to E3, but with less intense retroflection and a strong downstream meander. Only 4 rings are formed in 10 years, each of which requires a strong interaction with the subpolar front. |
| E11 | The boundary current is broader with smaller velocities than E10. The retroflection is still strong, but is less intense and there is a 5-10 Sv leakage. About 3 rings are formed per year, but not in such a regular fashion as in E1. |

3 THE VORTICITY BALANCE

3.1 Method of analysis

Taking an average over time, assuming statistical equilibrium, the full vorticity equation can be written

$$\underbrace{\overline{\vec{V} \cdot \nabla_s \zeta_s}}_{\text{RVA}} + \underbrace{\overline{\beta v}}_{\text{BETA}} + \underbrace{\overline{(\zeta_s + f)\nabla_s \cdot \vec{V}}}_{\text{STRCH}}$$

$$+ \underbrace{\overline{\vec{k} \cdot \left(\nabla_s \times \dot{s}\frac{\partial \vec{V}}{\partial s}\right)}}_{\text{VERT}} + \underbrace{\overline{\vec{k} \cdot \left(\nabla_s \alpha \times \nabla_s p\right)}}_{\text{SOL}}$$

$$+ \underbrace{\overline{A \operatorname{curl}_z \left(\left(\frac{\partial p}{\partial s}\right)^{-1} \nabla_s \cdot \left(\left(\frac{\partial p}{\partial s}\right) \nabla_s \vec{V}\right)\right)}}_{\text{VISC}} + \underbrace{\operatorname{curl}_z \left(\frac{\partial \tau_x}{\partial z}\right)}_{\text{WIND}} = 0$$

where s is the generalized vertical coordinate, density here; $\zeta_s$ is the relative vorticity evaluated at s=constant; $\operatorname{curl}_z$ is the vertical component of the curl; A is the constant horizontal eddy viscosity and the other symbols are conventional. (RVA) is the relative vorticity advection, (BETA) the planetary vorticity advection, (STRCH) the stretching term, (VISC) the viscous stress curl, (WIND) the wind stress curl, (SOL) the solenoidal term and (VERT) the curl of the vertical advection. The actual finite difference formulation of the vorticity equation which we use in computation of these terms conserves potential vorticity and potential enstrophy (see Bleck, 1979; Bleck and Boudra, 1981). Finding the mean values of the terms for the final five years of each experiment, a balance was obtained. Our computations have shown that SOL and VERT are zero or negligible. This can be expected from the use of isopycnal coordinates. In addition, STRCH is equal to zero in the one layer case and has very small temporal mean values in the multilayer case. It, therefore, is not addressed in our analysis.

3.2 The vorticity balance in a one-layer model

It is instructive to begin our discussion of the model vorticity balance with a weakly viscous, linear experiment. Removing the inertial terms from the equations of motion, the vorticity equation is simplified and the balance is among BETA, VISC and WIND. Our steady solution LIN1 (not illustrated here) has qualitatively the same characteristics as the analytical solution of De Ruijter (1982). Along the no-slip coast of Africa in the Munk layer, lateral friction balances the $\beta$-induced input of relative vorticity. The magnitude of the latter is determined by the southward velocity, which is governed by the

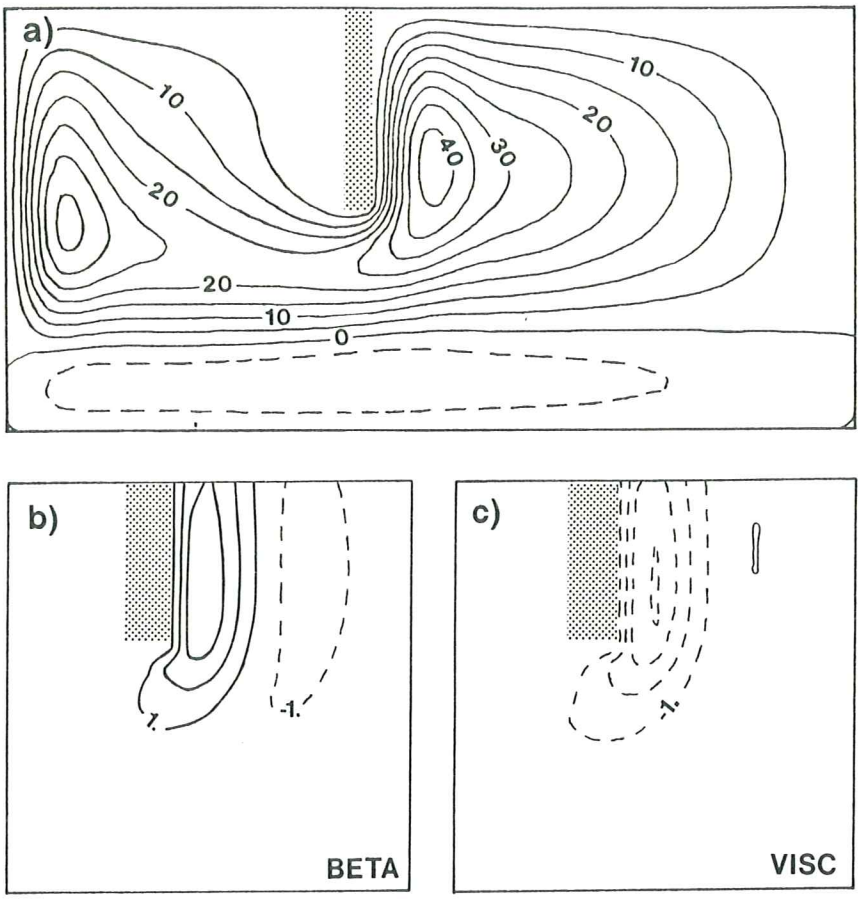


Fig.2. Experiment LIN2. (a) The mean mass transport streamfunction. The contour interval is 5 X $10^{6}m^{3}s^{-1}$. (b) The time mean distribution of planetary vorticity advection (BETA) around the southern tip of Africa. The contour interval is 2 x $10^{-12}s^{-2}$. (c) As in (b), except viscous stress curl (VISC).

combination of integrated wind curl and layer depth, as well as friction. In the low viscosity case (LIN1), the boundary layer is relatively thin and friction becomes very small after separation, and therefore, so does the planetary vorticity advection. The only way for the flow to satisfy this condition at the southern tip of Africa is to immediately turn westward or eastward. The wind curl maximum is only 120 km north of the latitude of Africa's tip. Therefore, there is very little linear return flow toward the Indian Ocean interior north of that latitude. Thus, most of the flow branches westward into the Atlantic.

If the viscosity is increased by an order of magnitude (LIN2) (Fig.2), friction becomes important in the area south of Africa. The current can continue southward for some distance since BETA (Fig.2b) can be balanced by VISC (Fig.2c). In other terms, the frictional boundary layer is broadened enough so that more streamlines of the separating Agulhas are able to connect with returning Sverdrup lines to the south and, thus, establish a partial retroflection. Important inertial effects are, therefore, not required in order to obtain retroflection; so that the latter may be obtained in highly diffusive, coarse-resolution models primarily because of the large lateral viscosity required by those models.

Introducing the inertial terms adds a new term to the vorticity balance, the relative vorticity advection RVA. Experiments NLIN1 (Fig.3) and NLIN2 (not illustrated here) correspond respectively to the nonlinear runs of LIN1 and LIN2. In the high viscosity case (NLIN2), most of the retroflection is moved south and west of the separation point, but the general characteristics of the flow pattern are unchanged. Inclusion of the inertial terms results in an increase in the diffusion of the negative relative vorticity. This is because the total velocity is a bit stronger and the boundary layer, now inertial-frictional, is thinner. BETA does not increase, however, since the orientation of the retroflection gains a SW-NE tilt. The increase in VISC is balanced by the new term RVA. The major conceptual difference from LIN2 is that the fluid may now flow southward from the tip of Africa due to its own inertia. Frictional effects are, however, still dominant.

In the corresponding low viscosity case (NLIN1) (Fig.3) where the boundary layer is relatively thin, friction is unimportant after separation and the effect of inertia is predominant. A substantial retroflection is still obtained as RVA now becomes the primary term to balance BETA. Inclusion of the inertial terms in the weakly viscous case substantially modifies the flow pattern and the

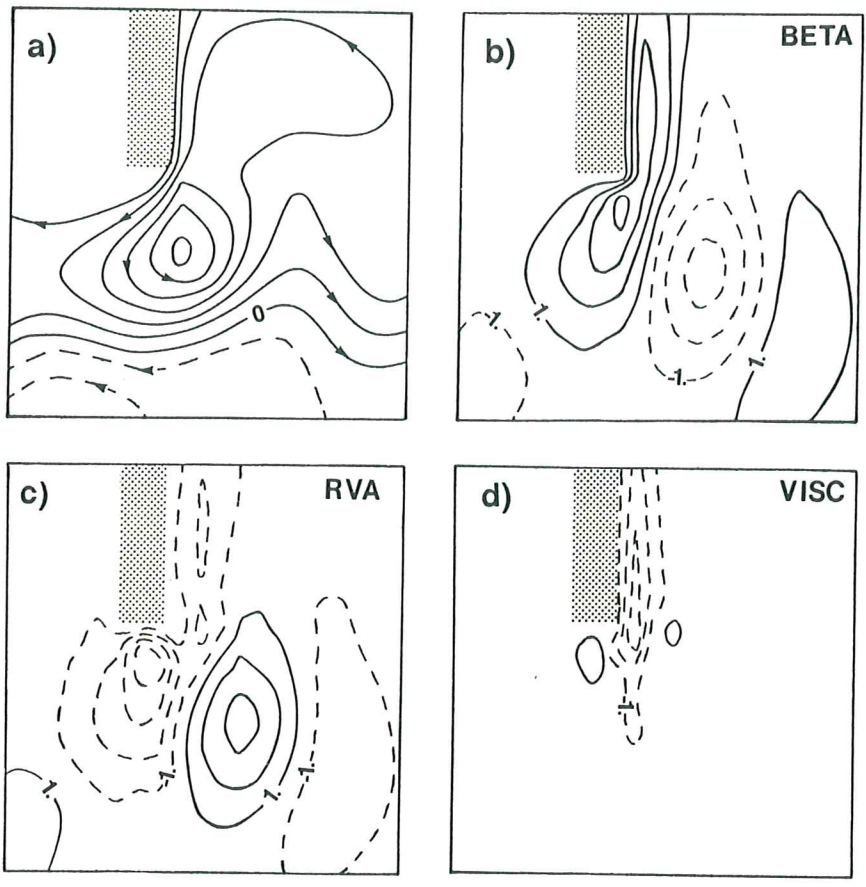


Fig.3. Experiment NLIN1. As in Fig.2 for (a) and (b). (c) Time mean distribution of relative vorticity advection (RVA). The contour interval is 2 x $10^{-12}s^{-2}$. (d) As in Fig.2c.

distribution of terms of the retroflection vorticity balance. The circulation east of Africa is southward intensified due to inertia, and weaker along the coast itself.

In each of LIN2, NLIN1 and NLIN2, there is a substantial retroflection. The similarity among all three is the establishment of a boundary layer after separation in which the beta effect is balanced by the turning eastward of a major portion of the current. In LIN2 the boundary layer is purely frictional, in NLIN2 it is inertial-frictional, and in NLIN1 it is a free inertial boundary layer. While the physical mechanism of retroflection is not the one proposed by De Ruijter (1982) -- the inertial overshooting distance -- his concept of the retroflection being accomplished within a free inertial boundary layer is

apparently applicable. In the experiments remaining to be discussed, the retroflection is accomplished in this free boundary layer. NLIN1 possesses a similar distribution of the terms as the weakly nonlinear multilayer cases and will be discussed further in parallel with them.

3.3 The vorticity balance in the multilayer model

(i) Variation of inertia. As described in BD, in experiments E1, E2 and E3, the strength of the retroflection depends on the inertia of the currents, which can be quantified by the Rossby number (Ro) of the overshooting boundary current. For E1 and E2, the top layer vorticity balance is similar to that for NLIN1 above (Fig.3). There is a change in the spatial distribution of the terms, however, for E3 (Fig.4). These experiments have high temporal variability, which is not the case in LIN1, LIN2 and NLIN2. RVA, therefore, can be separated into two components, one related to the mean flow and the other one to the transients. The RVA pattern is largely dominated by the component associated with the mean flow. However, the component due to the transients can have a canceling effect on that due to the mean flow, especially in NLIN1 and E1.

Along the coast of Africa and close to the boundary, viscous effects are important. Negative relative vorticity is generated by the no-slip boundary condition and then transported eastward by diffusion. BETA and VISC increase as Ro does from E1 to E3 and they balance each other. Away from the boundary, the effect of diffusion decreases and the balance is mainly between RVA and BETA.

Just after the flow leaves the coast, VISC is still important because the flow is strongly sheared. Before the separation, the southward velocity is maximum at the first grid point east of the coast. The viscous stress curl of such a profile has a minimum at this grid point. If the boundary current were very well resolved, a positive maximum in VISC would appear near the coast. As the current overshoots the tip of Africa, the current broadens and is better resolved by the grid lattice. A positive maximum does appear on the western side of the free jet, and this feature is present in most of the nonlinear experiments discussed (NLIN1, NLIN2, E1, E2, E3 and E10).

After separation, the experimental vorticity balances differ. Changes in VISC leave BETA dominant, leading to generation of positive relative vorticity. From here on RVA balances BETA. For each case, at least a portion of the current turns eastward into the Indian Ocean. On the westernmost side of the current, inertia is not strong enough to dominate the linear tendency, and this part of the flow drifts westward into the Atlantic. This leakage is very small in the high Rossby number cases, since only a very small part of the current's western edge has weak motion.

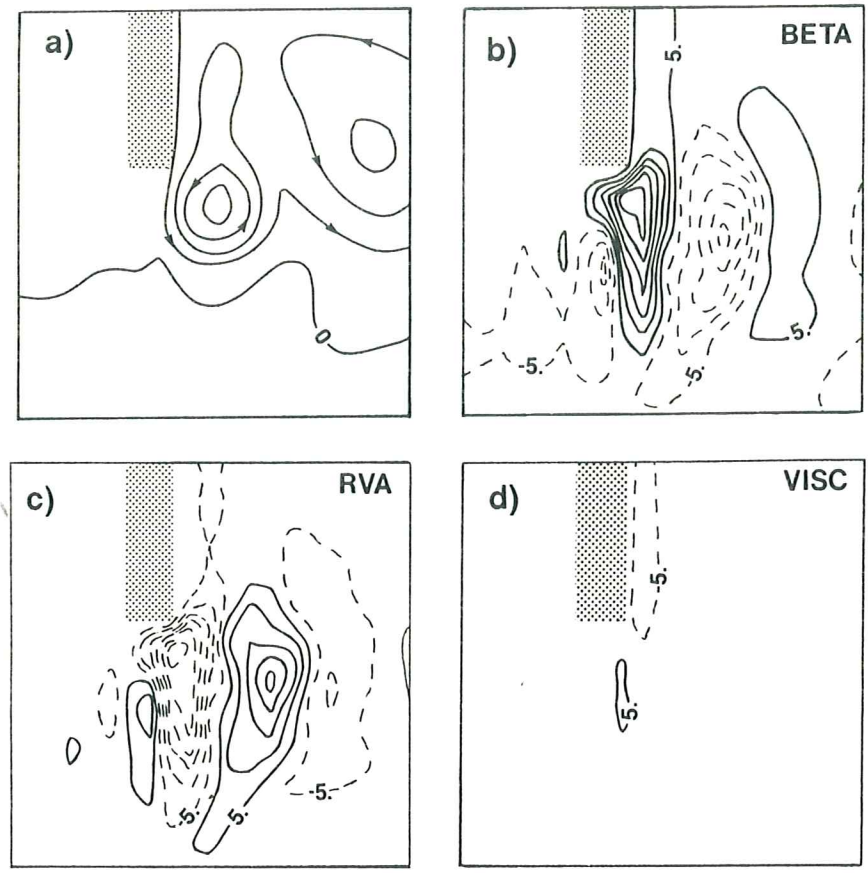


Fig.4. Experiment E3. As in Fig.3, except the contour interval in 10 X $10^{-12}$ $s^{-2}$ in (b), (c) and (d).

The planetary vorticity advection (BETA), proportional to the southward component of the velocity, is of primary importance in controlling the shape and the strength of the retroflection. As the Rossby number of the separating current increases, so does BETA and the tendency to turn eastward. Therefore, this turn moves closer to the tip of Africa as southward inertia increases, in contradiction to the inertial overshooting concept, and has no direct connection with the distance to the returning Sverdrup lines.

Inclusion of bottom drag in E8 (not illustrated here) decreases the eddy-induced mean circulation in the bottom layer, but increases the intensity of the upper layer circulation, since the bottom layer flow regime in E3 is a primary mechanism for draining energy from the retroflection area. In this experiment, the terms of the model vorticity balance are slightly larger in magnitude, but their horizontal distribution remains as in E3.

(ii) Horizontal resolution. As pointed out by BD, 40 km grid resolution cannot adequately describe the details of boundary layer flows. They performed E10 with grid spacing halved in order to test the sensitivity of the retroflection to improved resolution of the boundary layer and release of baroclinic instabilty. The retroflection flow pattern of E10 (not illustrated here) is similar to that of E8. In E10, the bottom layer circulation is revived by the improved resolution of instabilities and the upper layer circulation in the retroflection area is less intense than in E3 and E8. There is a similar horizontal distribution of the terms of the vorticity equation in E10 as in E3 and E8. BETA has a maximum near the coast as in E3, but VISC is even larger because the maximum velocity is greater and closer to the coast with the improved resolution. An additional contribution from RVA balances this enhanced VISC.

Regarding the principal balance the same conclusion as in Section 3.3.a can be drawn. As the current separates at the tip, VISC decreases and the remaining dominant term, BETA, generates positive relative vorticity. As in the 40 km resolution case, RVA balances BETA as the current turns eastward rejoining the Indian Ocean subtropical gyre.

(iii) Boundary condition along the African coast. BD obtained a very different two-basin flow configuration when a free-slip boundary condition along the coast of Africa was substituted for the no-slip condition. In the corresponding no-slip case (E8) only a small amount of fluid escapes into the Atlantic, the major part of the current retroflecting into the Indian Ocean. In the free-slip experiment, most of the fluid goes around the southern tip of Africa into the Atlantic.

In the top layer vorticity balance for E9 (not illustrated here), VISC is negligible in comparison to RVA and BETA along the coast and north of the tip of Africa. The principal balance is between these last two terms. Contrary to the no-slip case, there is no cyclonic vorticity present along the coast. The boundary layer is primarily inertial as opposed to the inertial-frictional boundary layer of the no-slip case. In order to overshoot the tip (and afterward retroflect), the current must coexist with a region beyond its western edge which is largely motionless. In the no-slip case, the western boundary condition for the current along the coast is already a motionless one and, thus, provided nonlinear effects are strong enough, the current shoots past the tip in a relatively natural fashion. In contrast, the condition at the western edge of the coastal current in E9 results in the current having its maximum velocity there. In an overshooting configuration it would have to adjust to a strongly sheared condition.

3.4 South African coastal geometry

The shape and orientation of Africa in the previous experiments is one which maximizes the importance of BETA in the model retroflection. Inasmuch as this term plays a dominant role, giving it a more realistic level of importance seems warranted. After leaving the South African coast, the real Agulhas flows along the Agulhas Bank shelf break, which is oriented approximately from northeast to southwest, before flowing out into deep water. In this configuration, the component of velocity advecting planetary vorticity is about 70% of the total, rather than 100%, as with the meridionally oriented coast of BD's model. The basin geometry shown in Fig.5a has been chosen, therefore, as a next step toward model realism.

The time mean top layer flow pattern (Fig.5a) for this 20 km resolution experiment (E11) bears many of the same characteristics as those of E10 (for comparison, see Fig.13 in BD). However, there are some notable differences, especially in the Indian Ocean sector. The retroflection is still strong, but less intense. The mean Agulhas along the coast is somewhat broader, and its maximum velocity is less than in E10. With the tilted coast, the energy of the boundary region has more of a tendency to leak into the Atlantic rather than to be trapped in the Indian Ocean.

The retroflection vorticity balance of E11 (Fig.5) is mostly similar to that in the high Rossby number rectangular geometry experiments with weak friction. Along the coast BETA (Fig.5b) and VISC (Fig.5d) essentially balance each other. Again, however, at certain points, VISC is particularly strong, and RVA makes up for what BETA does not supply there. Over the remainder of the retroflection, BETA and RVA (Fig.5c) are in balance. Incorporation of the more realistic geometry has no major impact on the retroflection vorticity balance. The magnitude of BETA at separation still requires an eastward turn and thus, retroflection.

Conspicuously absent from the diagram is the feature in VISC just beyond and to the west of the tip, which is present in the other multi-layer experiments discussed here. This is apparently because the coastal turn at separation is not nearly so sharp as with rectangular geometry and there is much more motion of fluid around this turn, principally within the rings drifting into the Atlantic. In fact, the retroflection of the Agulhas is usually upstream of the tip of Africa and the depicted flow pattern of Fig.5a averages through many ring formation events. The field of RVA exhibits a larger contribution from the transients than in E3, E8 and E10 because of the much greater frequency of ring formation. More details concerning the transient aspects of E11 are provided in Section 4.

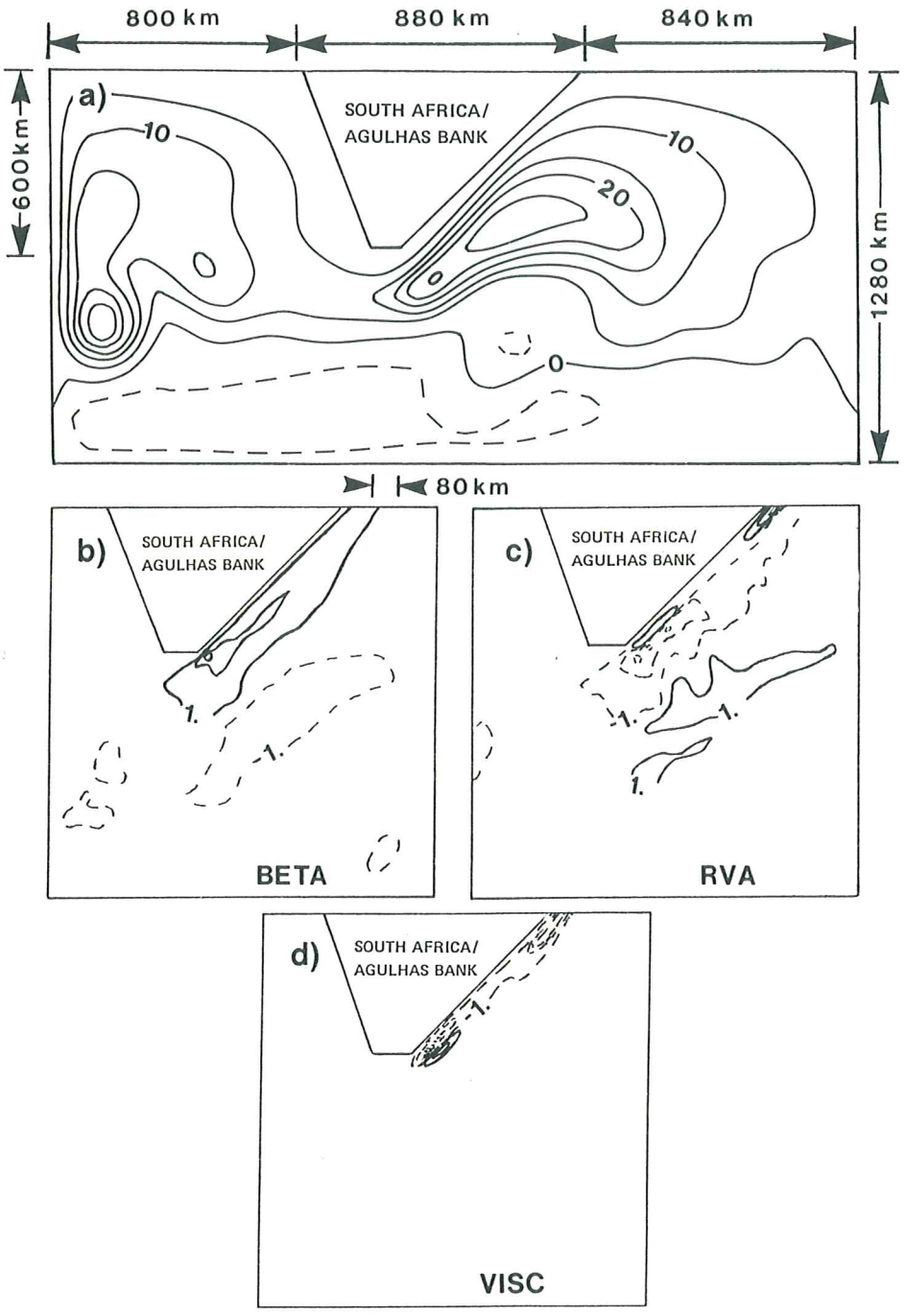


Fig.5. Experiment E11. (a) Upper layer mean mass transport streamfunction for the last five years. The C. I. is 5 x $10^6 m^3 s^{-1}$; (b), (c) and (d) as in Fig.3.

## 4 ENERGETICS AND RING FORMATION

### 4.1 Formulation of the energy conversion terms

A detailed derivation of the time mean and transient eddy energy conversion terms in isopycnic coordinates is given by Bleck (1985). Following his notation, they are as follows:

$$C(P,K_E): \quad \overline{\phi\nabla_s\cdot\left(\frac{\partial p}{\partial s}\,v'\right)}-\overline{v'\cdot\frac{\partial p}{\partial s}\,\alpha\nabla_s p}$$

$$C(P,K_M): \quad \overline{\phi\nabla_s\cdot\left(\frac{\partial p}{\partial s}\,\tilde{v}\right)}-\overline{\tilde{v}\cdot\frac{\partial p}{\partial s}\,\alpha\nabla_s p}$$

$$C(K_E,K_M): \quad \overline{v'\frac{\partial p}{\partial s}\cdot\left(v'\cdot\nabla_s+\dot{s}'\,\frac{\partial}{\partial s}\right)\bar{v}}$$

where $\phi$ is the geopotential; $(\bar{})$ is the time average; $(\tilde{})$ is the mass weighted time average; $(\,)'$ the departure from the mass weighted time average; $K_M$ is the kinetic energy associated with the mean flow and $K_E$, with the transient eddies; P is the total available potential energy and the other symbols are conventional.

Bleck (1985) showed that in the isopycnic framework a conversion term appears in the energetics suggesting an exchange between the eddy potential energy and $K_M$. To avoid confusion, therefore, P is not decomposed into mean and eddy components. It is assumed that the exchange between P and $K_E$ is associated with baroclinic conversion and that the transfer from $K_M$ to $K_E$ is associated with barotropic conversion.

### 4.2 Mean energetics

In order to gain some additional insight into the impact of the model parameters most influential on the retroflection, we now examine the mean energetics of some of the experiments discussed above, illustrated in box diagram form in Fig.6. The time means of the energies and conversions terms are computed over the last five years of a ten year run for E1, E2, E3, E8, E9 and E11 and over selected years for E10.

Considering the influence of inertia on the basin averaged energetics, we first compare E1 and E2. The layer receiving most of the direct wind forcing is thinner in E2 than in E1, leading to increased kinetic energy in the boundary

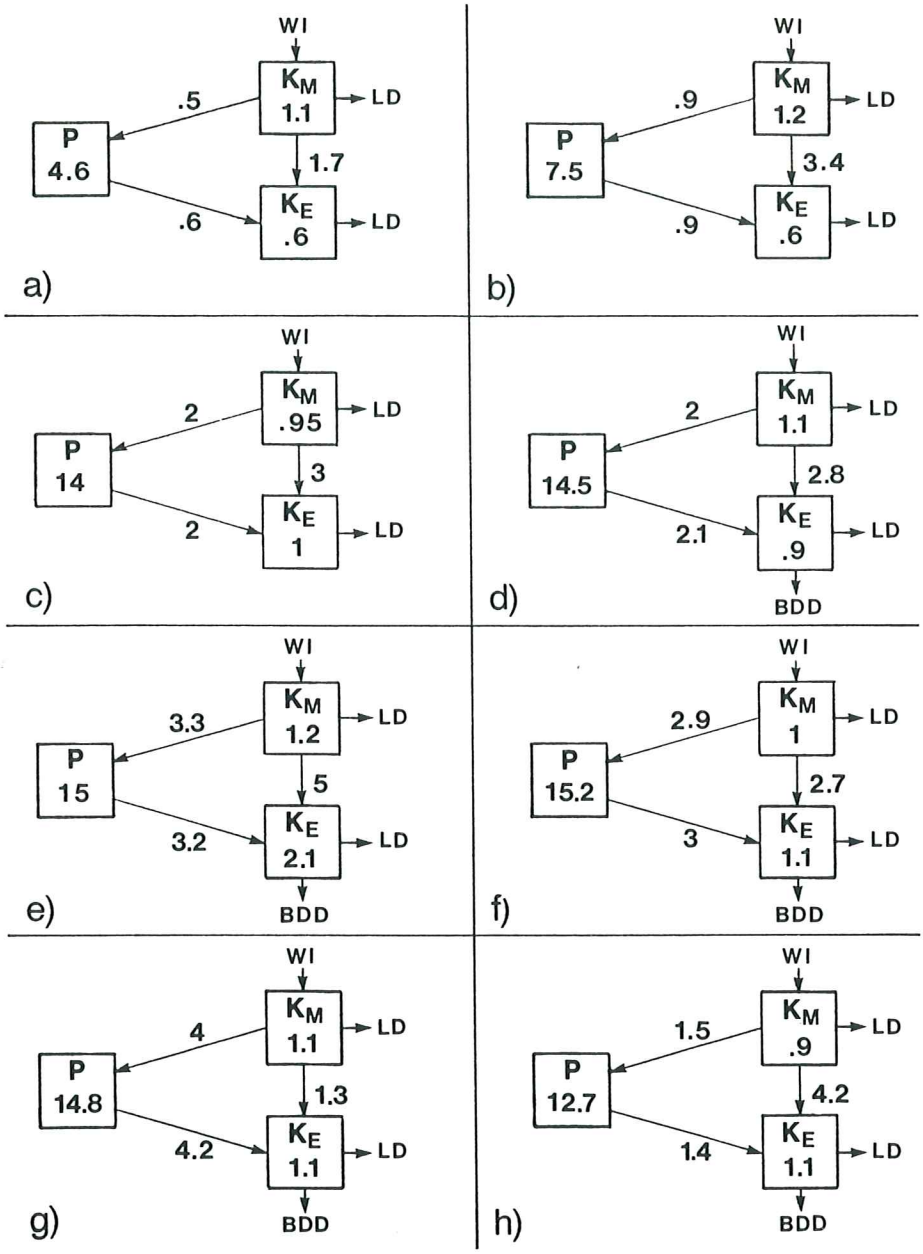


Fig.6. Eddy-mean energetics for (a) E1; (b) E2; (c) E3; (d) E8; (e) E9; (f) E10, year 4; (g) E10, year 7; (h) E11. WI is the wind input; LD, the lateral dissipation and BDD the bottom drag dissipation.

currents, even though the basin average kinetic energy does not change much (Fig.6a,b). As the top layer flow increases in speed, so does the vertical shear. From the thermal wind relation, this leads to more strongly tilted isopycnal surfaces and, thus, to more energy exchange between $K_M$ and P. The available potential energy, however, is distributed over the whole domain, as opposed to the kinetic energy, which is concentrated mostly in the boundary currents (Fig.3 of BD). In the basin averaged sense, then, this parameter has a much larger impact on the potential energy than on the kinetic energy. Horizontal plots show that most of the conversion from $K_M$ to $K_E$ occurs in the retroflection area. Rings are continuously being formed there and, therefore, the increase in strength of the boundary currents from E1 to E2 apparently results in an increase in kinetic energy exchange between the mean flow and the eddies in this highly transient region.

The upper layer is thinner yet in E3 (Fig.6c), so that inertia is even greater in the boundary currents, leading to an increase of 300% in available potential energy from E1. This increase is accentuated by the fact that the circulations in the subtropical Indian and Atlantic oceans are almost separated. The boundary currents' kinetic energy increases, but no rings are formed in this experiment, and so there is less conversion between $K_M$ and $K_E$ than in E2, even though there is substantially more $K_E$ in E3. Inclusion of bottom drag in E8 (Fig.6d) increases dissipation in the bottom layer. As mentioned in Section 3.3, this leads to a more stable and intense retroflection in the upper layer. Therefore, there is less $K_E$, but the conversions are essentially as in E3.

In the free-slip case (E9) (Fig.6e), the total kinetic energy is 50% higher than in E8, primarily because of the reduction of kinetic energy dissipation along the coast of Africa. The boundary currents and the free jet in the South Atlantic become stronger, and through geostrophic adjustment, P and the exchange between kinetic and potential energies increase also. The flow regime is particularly turbulent south of Africa in this experiment leading to large values of $K_E$ and $C(K_M,K_E)$.

The increased horizontal resolution of E10 better represents the release of baroclinic instability. Increases are noticed in P, and in the potential to kinetic energy conversions because the boundary currents are even stronger than in E3 and E8. Since four rings were formed during the ten year experiment, it is also interesting to note the difference in the energetics for years with and without ring formation. In the latter case, the $K_M$-P-$K_E$ appears to be the primary energy path (Fig.6f). During a year with a ring, the baroclinic and barotropic transfers are of the same order of magnitude (Fig.6g). This comparison strongly suggests the association between $C(K_M,K_E)$ transfer and formation of a ring. Supporting this assertion is the fact that the change in

South Africa' s geometry (E11) results in more barotropic conversion. In fact, the dominant transfer is the one from $K_M$ to $K_E$ (Fig.6h). The major difference between the two experiments is the much greater number of rings formed in E11. Also, P is approximatively 15% smaller in E11 than in E10 because the retroflection is less intense and the Agulhas along the boundary is somewhat broader.

The question arises as to whether basin-averaged energetics are truly relevant in discussing the dynamical processes in the retroflection region. Harrison and Robinson (1978) showed that energy transfer averaged over a model domain may not be characteristic of any important subregion. BD showed, however, that especially in the high Rossby number experiments, most of $K_M$ and $K_E$ are localised in the retroflection area. Our calculations have shown that almost all the $C(K_M,K_E)$ is in the Agulhas region and $C(P,K_E)$ is maximum in this region. Therefore, the energetics averaged over the whole basin give a good indication of events occuring in the retroflection area for these cases.

4.3 Ring formation

Agulhas rings have been observed and studied by Gordon (1985) and Olson and Evans (1986). Lutjeharms (1981) was able to capture the formation of one ring in an analysis of satellite imagery, but little has been established about the frequency of their formation and about the dynamics that drive the shedding, mostly because the rings are strongly nonlinear features. For example, might the formation of the rings and the associated leakage be strongly influenced by seasonal factors (wind-stress or inflow) or by nonlinear oscillations of the recirculation region off South Africa? Observational efforts to find time-dependence in the Agulhas Current transport by Pearce and Grundlingh (1982) were not conclusive and, in our model, rings form with constant forcing. In their study of the dynamics of the loop current and eddy shedding of the Gulf of Mexico, Hulburt and Thompson (1980) obtained a similar result with a quasi-annual eddy shedding. Even with realistic time variation of the upper-layer inflow, the eddy-shedding period was dominated by the quasi-annual period rather than by the forcing period, although the influence of the latter was not negligible.

In order to get some understanding of ring formation in the model, we describe a typical event of E11, illustrated here in Fig.7. In the upper layer, at day 2950 (Fig.7a), the flow pattern is in a quasi-steady configuration. An already formed ring is centered just southeast of the tip of Africa and the retroflection of the Agulhas proper is a short distance up the coast. Thirty days later, the meander east of the retroflection has begun to amplify and the center of the retroflection is moving southwest (Fig.7c). The already formed ring has begun moving toward the Atlantic. The lower layer at day 2950 shows a

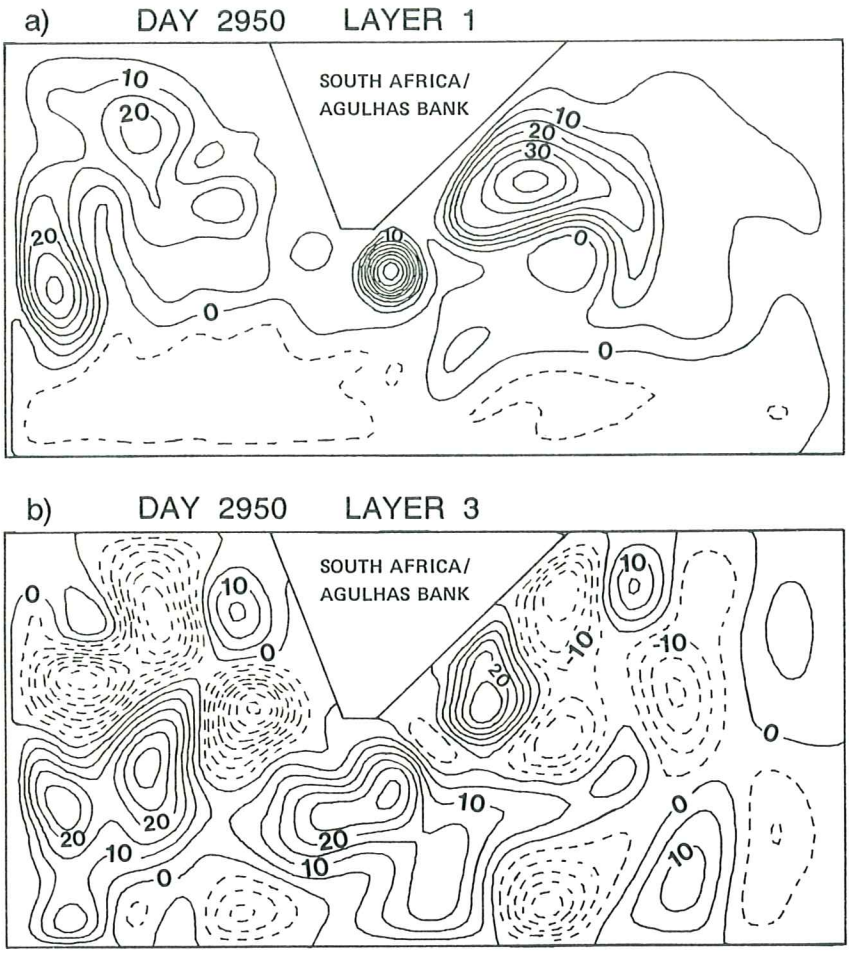


Fig.7. Ring formation in E11. Upper and lower layer mean mass transport streamfunctions. The contour interval is 5 x $10^6 m^3 s^{-1}$.

couplet of cyclonic gyres located under the meander (Fig.7b). As the amplitude of the upper layer meander grows, they merge and intensify (Fig.7f). This intensification reaches a maximum when the ring cuts off. Its intensity weakens rapidly thereafter (Fig.7j).

The dramatic growth of this cyclonic circulation in the third layer is suggestive that baroclinic instability is being released during ring formation. In his recent model study of the Gulf of Mexico Loop Current, Hulburt (1986) also found that an intense cyclonic circulation develops in the lower layer when an eddy is shed. In order to get more insight into the instabilities involved,

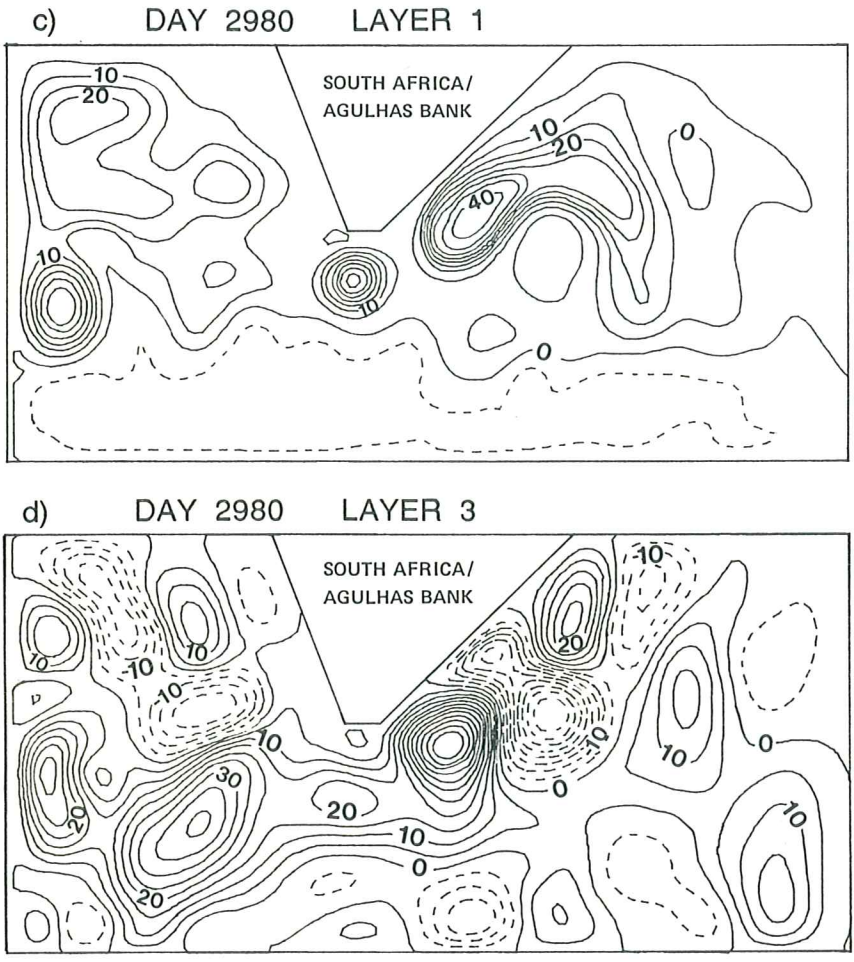


Fig.7. (Continued)

we now look at the time evolution of the energy conversion terms during this and the subsequent event (Fig.8). The mean components in the energetics are averaged over a year. The two strong signals in $C(K_M,K_E)$ in Fig.8 correspond to the two events of ring formation. In both cases, before the meander begins to grow, the baroclinic conversion term is negative. Then, as the amplitude of the meander increases, $C(P,K_E)$ rises above zero and reaches a maximum when the ring is formed. The barotropic conversion term is larger and reaches a maximum at the same time. It is not clear, however, that $C(K_M,K_E)$ is directly related to barotropic instability. Possibly, it is simply suggestive that kinetic energy which has been residing in the time mean flow field is being transfered into a

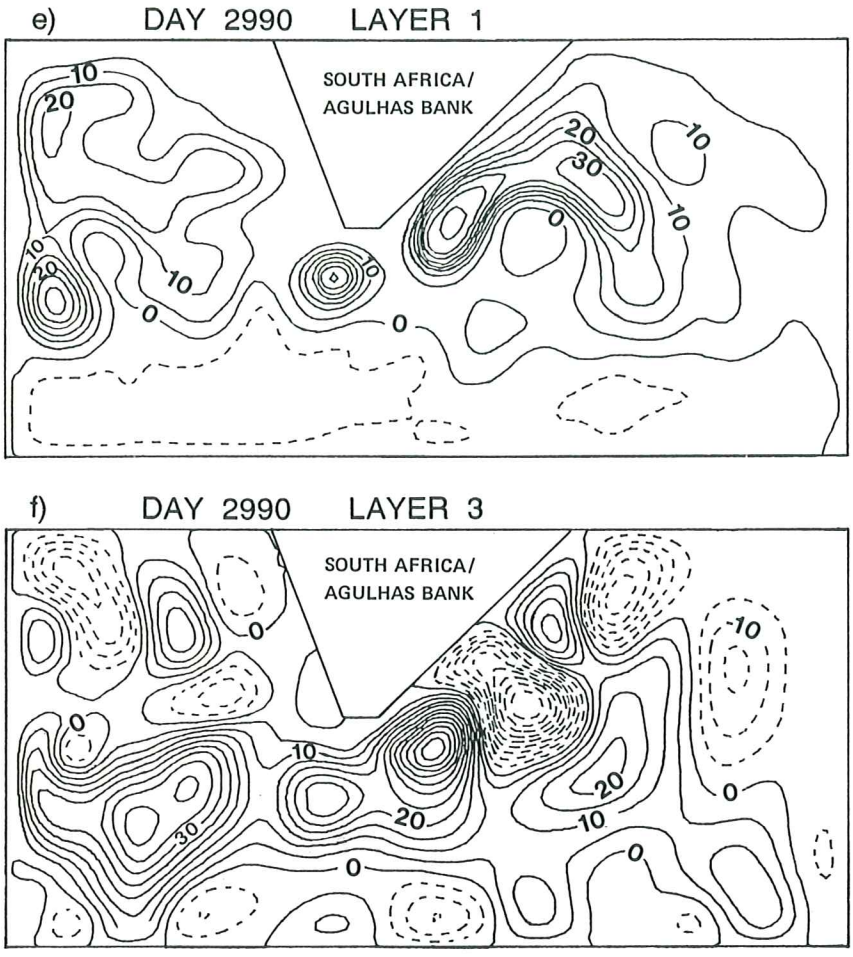


Fig.7. (Continued)

different flow configuration. Therefore, no conclusion can be reached as to whether barotropic or baroclinic instability is dominant. We can only say that both barotropic and baroclinic conversions have significant peaks during ring formation. It would appear that the instability is of the mixed type.

The character and frequency of ring formation in the experiments depend on the choice of parameters, as shown in Table 2. Analysis of the vorticity balance in Section 3 showed how important is the magnitude of the planetary vorticity advection in the strength of the retroflection. As the Rossby number of the boundary currents is increased, more fluid retroflects and fewer rings are formed. With 40km grid resolution, rings are formed in the low Rossby

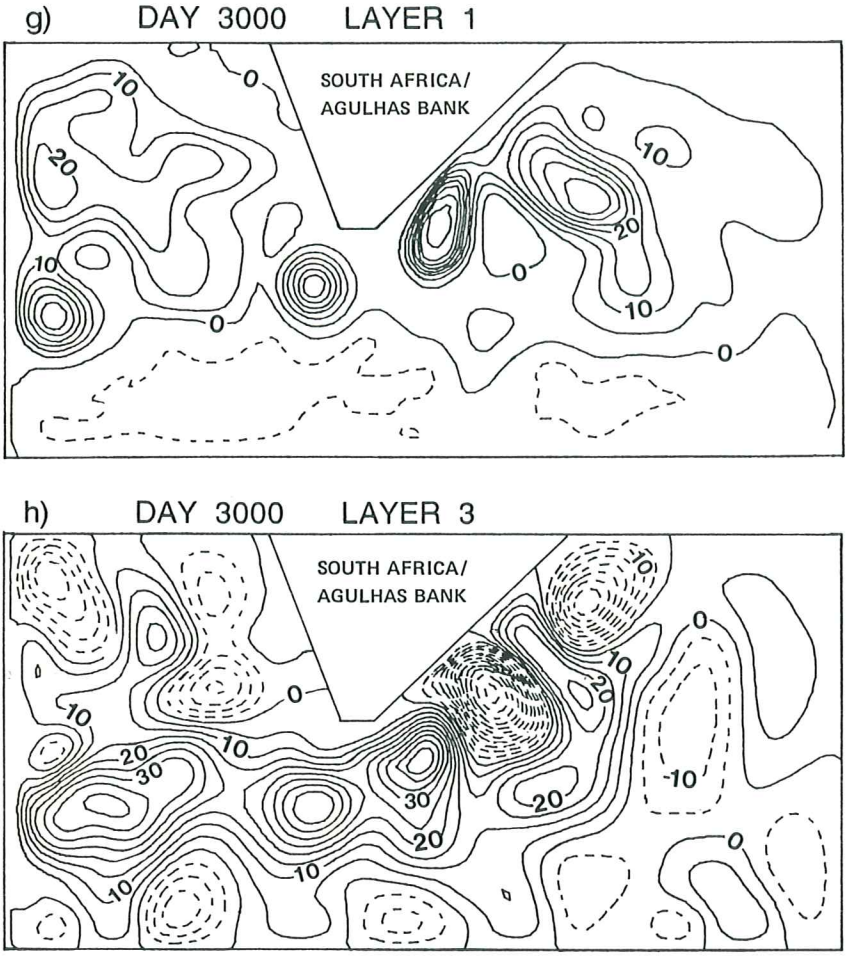


Fig.7. (Continued)

number cases (E1 and E2) and none in the high Rossby number cases (E3 and E8). But in the latter case, a change in the geometry of Africa in which the retroflection is less intense (same as E11 with 40km grid resolution, not presented here) leads to formation of rings. A few rings were also formed with an increase in horizontal resolution (E10) in which the release of baroclinic instability is improved.

The analysis of rings formed in E1 and E10 supports the result found in E11. In both experiments, as shown in Fig.9 and Fig.10 respectively, $C(K_M,K_E)$ and $C(P,K_E)$ reach maxima of the same magnitude at the moment of ring formation. As in E11, a cyclonic circulation develops in the lower layer and reaches maximum

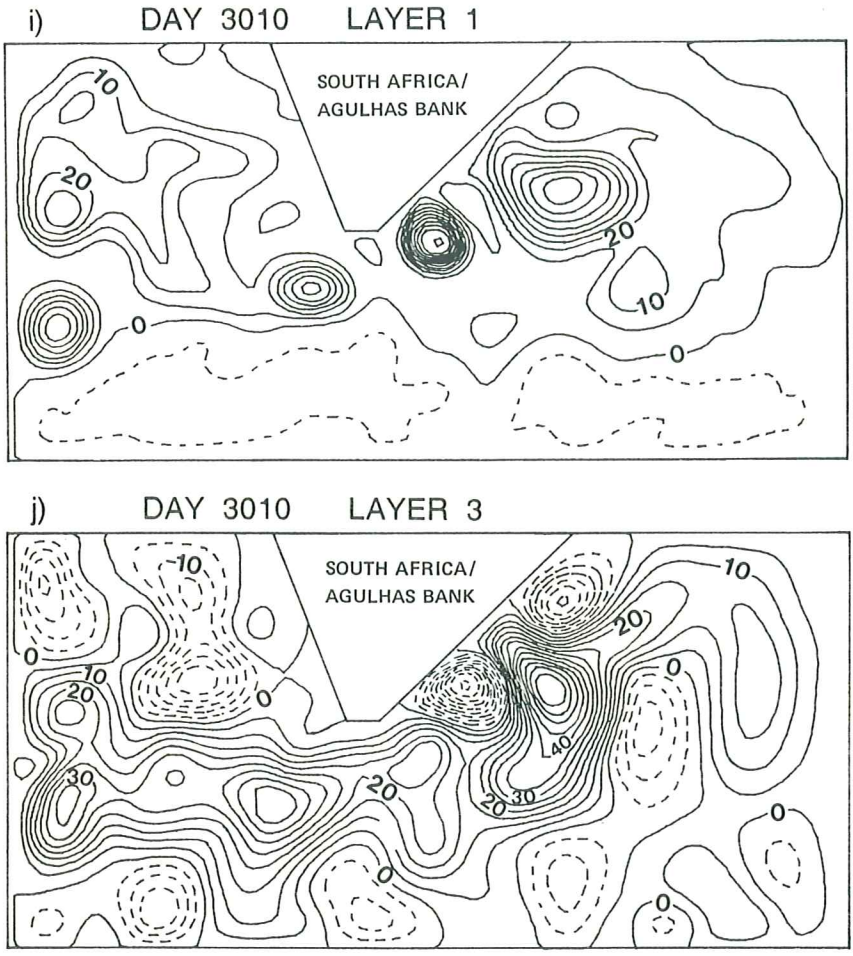


Fig.7 (Continued)

intensity when the ring separates from the gyre. To conserve space here, instantaneous streamfunctions for those two experiments are not presented. In E1, rings are formed in a continuous manner at the southern tip of Africa at a rate of about five per year. As soon as an already formed ring begins to drift toward the Atlantic, the center of the retroflection moves southward and shortly thereafter a new ring cuts off. The two peaks in Fig.9 correspond to two consecutive events of E1 in year 9. The formation process is quite different in E10, where only four rings are formed in ten years. The core of the Agulhas Current possesses more planetary vorticity advection than in E1. In E10, for a ring to cutoff, the center of the retroflection must be rather far south and a

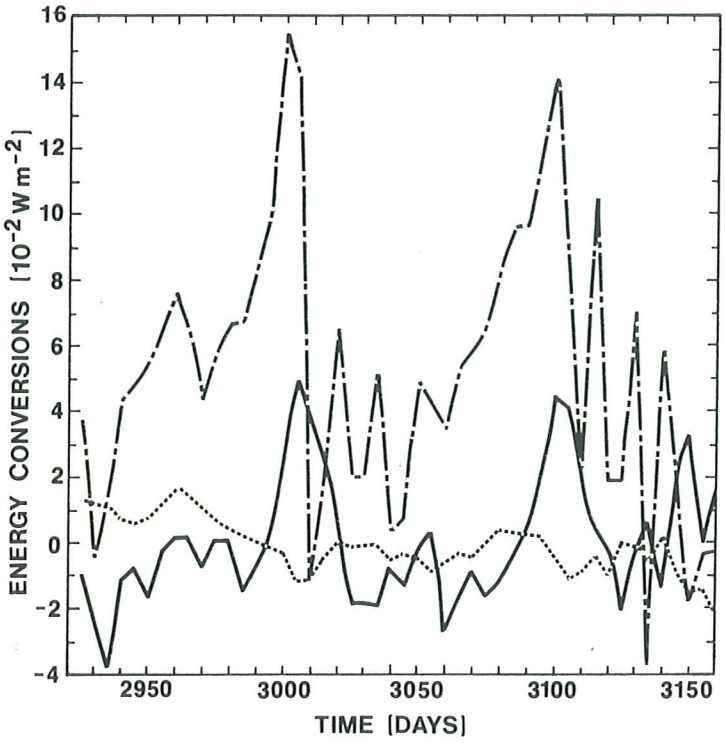


Fig.8. Experiment E11. Variations of the energy conversion terms with time. The dashed-dotted line corresponds to $C(K_M, K_E)$, the solid line to $C(P,K_E)$ and the dotted line to $C(P,K_M)$. Rings are formed at day 3000 and 3100.

dome of low potential vorticity fluid from the subpolar gyre must intrude northward along the east side of the retroflection region. In addition, the front between the gyres needs to be far enough south so that the cutoff ring can escape into the Atlantic before being recaptured by the Agulhas. For the event presented in Fig.10 occuring at the beginning of year 9 (illustrated in Fig.14 of DB), the first peak in $C(K_M,K_E)$ corresponds to the initial ring cut off, the second one to a temporary reabsorption and the third one to the final cut off of the ring. No baroclinic conversions are associated with the last pinching off.

## 5 SUMMARY

The vorticity balance, the mean energetics and energy conversions have been used as tools with which to describe the dynamics of Agulhas retroflection and ring formation in a quasi-isopycnic coordinate numerical model. In addition, analysis of some new experiments has increased understanding of the model

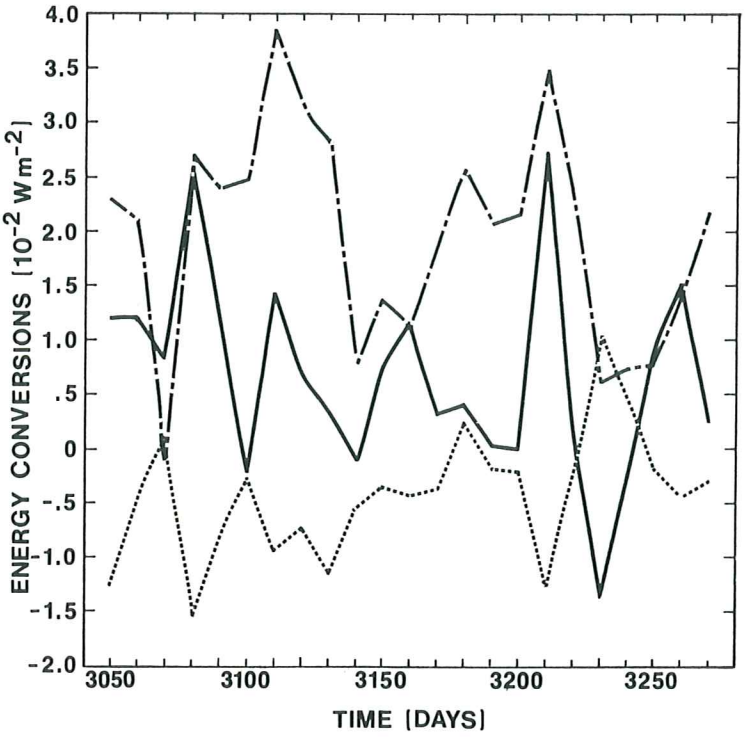


Fig.9. As in Fig.8 for experiment E1. Rings are formed at day 3080 and 3210.

parameters most influential in the retroflection.

The analysis of the vorticity balance of a one-layer simplification of the Bleck and Boudra (1981) numerical model in an idealized South Atlantic-Indian Ocean basin showed that either strong internal friction or inertia can bring about a partial retroflection where a linear model with weak friction has none. With the full quasi-isopycnic coordinate model, it was first shown how important is the magnitude of the planetary vorticity advection in the strength of the retroflection. As the Rossby number of the boundary currents is increased, more fluid retroflects and retroflects earlier after separation. When horizontal resolution is doubled to better resolve the boundary currents and instabilities, the magnitude of the terms of the vorticity balance increases as the current becomes narrower and its maximum velocity increases. Otherwise, the balance is unchanged. The importance of the frictional boundary condition was brought out through a no-slip/free-slip comparison. A new South African geometry was also adopted, in which the planetary vorticity advection is less important. The retroflection was shown to be less intense, but the primary balance is unchanged.

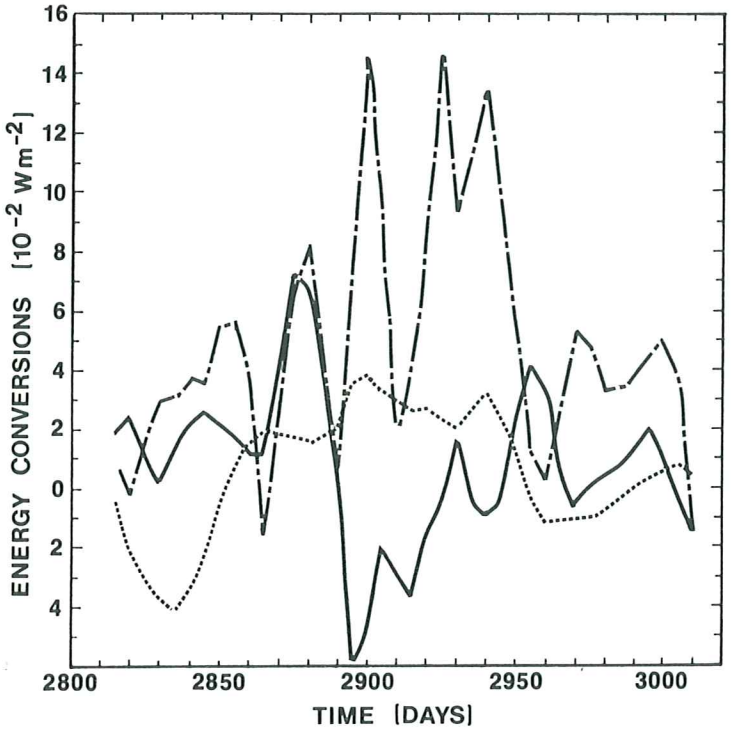


Fig.10. As in Fig.8 for experiment E10. The ring is formed at day 2880, then reabsorbed at day 2900. The final cutoff occurs at day 2930.

Additional insight on the model retroflection was gained through an analysis of the mean energetics of the experiments. It was shown that as inertia increases, more kinetic energy is present in the boundary currents, even though the basin averaged kinetic energy does not change much. This leads to more strongly tilted isopycnal surfaces and to more energy exchange between $K_M$ and P. Energy exchange between $K_M$ and $K_E$ is especially large in those experiments in which rings are formed often. As the Rossby number of the boundary currents increases, more fluid retroflects and fewer rings are formed. Events of three experiments were examined in detail. Certain aspects of ring formation are different among the experiments, but each exhibits a maximum in $C(K_M,K_E)$, $C(P,K_E)$ and a pronounced cyclonic development in the lower layer when a ring cuts off. While both barotropic and baroclinic conversions have peaks, whether one principal form of instability leads to ring formation is not clear. Instability of the mixed type seems more likely.

ACKNOWLEDGEMENTS

We wish to acknowledge helpful discussions with Prof. Claes Rooth and Prof. Rainer Bleck's assistance in clarifying the finite difference form of the model vorticity equation. This work has been supported by the Office of Naval Research Contract No. N00014-85-C0020. Computations were performed using the Cray-1 computers at the National Center for Atmospheric Research, which is sponsored by the National Science Foundation.

REFERENCES

Bleck, R., 1979. Finite-difference equations in generalized vertical coordinates. Part II: Potential vorticity conservation. Contrib. Atmos. Phys., 51, 360-372.

Bleck, R., 1985. On the conversion between mean and eddy components of potential and kinetic energy in isentropic and isopycnic coordinates. Dyn. Atmos. Oceans, 9, 17-37.

Bleck, R., and Boudra, D.B., 1981. Initial testing of a numerical model ocean circulation model using a hybrid (quasi-isopycnic) vertical coordinate. J. Phy. Oceanogr., 11, 755-770.

Boudra, D.B., and de Ruijter, W., 1986. The wind-driven circulation in the South Atlantic-Indian Ocean. II. Experiments using a multi-layer numerical model. Deep-Sea Res., 33, 447-482.

de Ruijter, W., 1982. Asymptotic analysis of the Agulhas and Brazil Current system. J. Phys. Oceanogr., 12, 361-373.

de Ruijter, W., and Boudra, D.B., 1985. The wind-driven circulation in the South Atlantic-Indian Ocean. I. Numerical experiments in a one-layer model. Deep-Sea Res., 32, 557-574.

Gordon, A.L., 1985. Indian-Atlantic transfer of thermocline water at the Agulhas Retroflection. Science, 227, 1030-1033.

Harrison, D.E., and Robinson, A.R., 1978. Energy analysis of open regions of turbulent flows - mean eddy energetics of a numerical ocean circulation experiment. Dyn. Atmos. Oceans, 2, 185-211.

Hulburt, H.E., and Thompson, J.D., 1980. A numerical study of Loop Current intrusions and eddy shedding. J. Phys. Oceanogr., 10, 1611-1651.

Hulburt, H.E., and Thompson, J.D., 1982. The dynamics of the Loop Current and shed eddies in a numerical model of the Gulf of Mexico. Hydrodynamics of semi-enclosed seas. By J.C.J. Nihoul (ed.), 243-298.

Lutjeharms, J.R.E., 1981. Spatial scales and intensities of circulation of the ocean areas adjacent to South Africa. Deep-Sea Res., 28a, 1289-1302.

Olson, D.B., and Evans, R.H., 1986. Rings of the Agulhas. Deep-Sea Res., 33, 27-42.

Pearce, A.F., and Grunlingh, M.L., 1982. Is there a seasonal variation in the Agulhas Current? J. Mar. Res., 40, 177-184.